Available online at www.sciencedirect.com
ScienceDirect
Trans. Nonferrous Met. Soc. China 32(2022) 3334−3348
Transactions of Nonferrous Metals Society of China
www.tnmsc.cn

Effects of TaN nanoparticles on microstructure, mechanical properties and tribological performance of PEEK coating prepared by electrophoretic deposition

Lin CAO[1], Peng ZHANG[1,2], Shuang-jian LI[1,2], Qi-wei WANG[1], Da-hai ZENG[1], Chuan-yong YU[1], Qing-yang LI[1], Yu-wen LIAO[1], Zhi-dan LIN[1], Wei LI[1]

1. Institute of Advanced Wear & Corrosion Resistant and Functional Materials, Jinan University, Guangzhou 510632, China;
2. Shaoguan Research Institute of Jinan University, Shaoguan 512027, China

Received 25 August 2021; accepted 30 December 2021

Abstract: In order to solve the friction, wear and lubrication problems of titanium, a series of TaN/ployether−ether−ketone (PEEK) coatings were developed by electrophoretic deposition, and the effects of TaN nanoparticles on the microstructure, mechanical properties and tribological performance of coatings were explored. Results manifest that the introduction of TaN nanoparticles into PEEK coatings could improve the deposition efficiency, enhance the resistant deform capacity, increase the hardness, elastic modulus and adhesive bonding strength. Compared with the pure PEEK coating, the friction coefficient of P-TN-3 was greatly reduced by 31.25%. The wear resistance of P-TN-3 was also improved in huge boost, and its specific wear rate was decreased from 9.42×10^{-5} to 1.62×10^{-5} $mm^3\cdot N^{-1}\cdot m^{-1}$. The homogeneous composite TaN/PEEK coatings prepared by electrophoretic deposition were well-adhered to the titanium alloy substrate, TaN nanoparticles could improve the strength of PEEK coating, and provide wear-resistance protection for titanium alloys.

Key words: ployether−ether−ketone coating; tantalum nitride; particle reinforcement; microstructure; mechanical properties; biotribology

1 Introduction

Because of their remarkable mechanical properties, corrosion resistance, passivity, and biomedical properties, titanium alloys have been the focus implant materials for load-bearing applications, hard tissue replacement, and fracture healing [1−4]. Despite the advantages of titanium implantable materials, their poor tribological performance is still a significant cause of concern for materials scientists and biomedical engineers. The principal reason for this concern is that plenty of wear debris due to relative movement of implants surface damage would interact with the surrounding aggressive environment and cause the immunological responses of surrounding tissues, eventually resulting in infection and aseptic loosening [5].

Extensive efforts have been made to solve the problem. The poor tribological properties of titanium implant could be improved by a efficiently protective coating via proper surface engineering technologies [6−8]. Conventionally, the “hard” coatings could enhance the wear resistance by surface strengthening and the “soft” coatings could reduce the wear by self-lubricating. Among hard coatings, TiN hard coating is thought to be effective

Corresponding author: Zhi-dan LIN, Tel: +86-20-85220890, E-mail: linzd@jnu.edu.cn;
Wei LI, Tel: +86-20-85223562, E-mail: liweijn@aliyun.com
DOI: 10.1016/S1003-6326(22)66051-5

in relieving abrasive and adhesive wear [9], TiO_2 coating is another hard one for better tribological performance [10,11], and WC coatings combine advantages of the excellent wear resistance and low friction coefficient [12]. These hard coatings could reduce scratching and offer good load-carrying capacity for protecting the titanium. Nevertheless, hard coatings are always relatively expensive and difficult to prepare, whose high roughness may also cause decreasing adhesive strength [13]. Moreover, because of ultra-high hardness of hard coatings, the improvement of tribological performance may be at the expense of increasing wear damage to their friction pairs. Besides, the hard coatings contain inherent brittleness and low fracture toughness, which are significantly limited for load-bearing applications [14]. Therefore, developing coating with low shear strength, strong adhesion and high bearing capacity has become one of the focuses of protecting titanium implantable materials from overwearing [15].

With relatively low friction coefficient, good biomedical properties, inexpensive and easy to fabricate, polyether−ether−ketone (PEEK) and PEEK-based composite coatings have been highly focused on recently [16−18]. But for biomaterials candidates, the poor strength of PEEK needs to be improved for cyclic load bone implant application. Therefore, many strategies have been developed to optimize the PEEK material composition to improve its mechanical performance [19−21]. Extensive research has shown that particle reinforcement PEEK could improve the properties of the titanium alloys effectively. Among these enhancing particles, TaN has more outstanding characteristics and can be used in the medical field. LENG et al [22] reported a TaN coating with excellent blood compatibility. Besides, ZHANG et al [23] found that TaN coating was beneficial to improving the hardness and elastic modulus of pure titanium, and could also improve the resistance of titanium alloys to microbial induced corrosion, which indicate that TaN could be used to modify hard tissue implants.

Bearing the above perspective in mind, herein, a series of TaN/PEEK coatings were designed. The advantages of electrophoretic deposition (EPD) treatment (TiN, Si_3N_4, Al_2O_3) on titanium and titanium alloys have been widely reported in the last years, but few studies declared the TaN reinforcement PEEK composite coating [24−26]. The coatings were thoroughly analyzed to understand the tribological mechanisms from the nanoparticles, the enhancement effect, the structure, the nanohardness, the elastic modulus, the H/E (H is the hardness, and E is the elastic modulus), and the H^3/E^2 ratio. The main objectives of this work were to investigate the possible roles of the TaN/PEEK composite coatings on micro-structure, mechanical properties and tribological performance of titanium-based alloys, and explore a potential design route of titanium-based medical materials surface modification for longer lifespan and better safety issues.

2 Experimental

2.1 Processing

Titanium plate (purity >99.999%, Dongguan Yanxin Metal Products Co., Ltd., China) with dimensions of d27 mm × 3 mm was used as the substrate. PEEK powder (purity > 99.99%, particle size: ~25 μm, 550UPF, Jilin Zhongyan Polymer Material Co., Ltd., China), and TaN powder (purity >99.5%, particle size: ~260 nm, Aladdin Industrial Corporation, Shanghai, China) were chosen as the raw materials for preparing the composite coating. The morphologies of PEEK and TaN particles are shown in Fig. 1. The PEEK

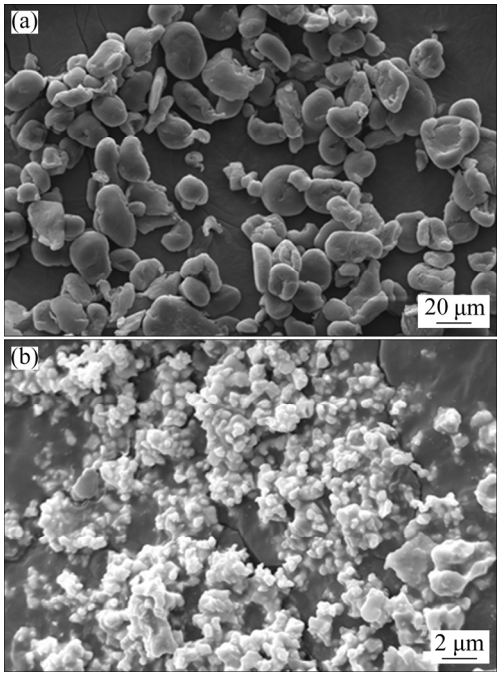

Fig. 1 SEM images of PEEK (a) and TaN (b) particles

particles show an irregularly flattened morphology. And the size of TaN particles was in nanoscale, which owned large specific surface area and high surface energy, and were easy to agglomerate. The suspensions consisted of as-prepared PEEK powders in 100 mL electrophoretic deposition solution (50 mL ethanol, and 50 mL chitosan solution containing 5 mL acetic acid and 0.1 wt.% chitosan). The surface potentials of the PEEK and TaN particles were modified with chitosan as dispersants. These particles would be modified positively charged, and improve the deposition efficiency. The solutions would finally be mixed with different mass fractions of TaN nanoparticles (0, 1.31, 3.23, and 6.25 wt.%), stirring until well combined as four kinds of electrolytes. Table 1 shows abbreviations and detailed compositions of the coating specimens.

The EPD solution was sonicated for 30 min, and magnetically stirred for 30 min, respectively. To avoid the settlement of particles, the mixture was continually stirred during the deposition process. The electrophoretic deposition power source was IT6720 (ITECH Electronic Co., Ltd., Nanjing, China). The deposition process was carried out by utilizing two-electrode system, of which a platinum (Pt) slice acted as an anode and the titanium (Ti) matrix as a cathode. The spacing between the cathode and anode fixation distance was 1 cm. Then, electrophoresis was conducted for 30−180 s at 15−25 V. The electrodes were weighed before and after the deposition in order to calculate the mass of the nanocomposite coating. And the relationships among deposition mass, time and voltage are shown in Fig. 2.

Table 1 Abbreviations and compositions of PEEK specimens investigated

No.	Abbreviation	PEEK content/wt.%	TaN content/wt.%
1	PEEK	100	0
2	P-TN-1	98.69	1.31
3	P-TN-3	96.77	3.23
4	P-TN-6	93.75	6.25

All heat treatments were conducted in a tubular furnace. The titanium matrices with different composition coatings were heated to 390 °C at a rate of 4.5 °C/min, and remained constant for 60 min. Macroscopic images of different coatings before and after sintering are shown in Fig. 3. The color of the sample surface

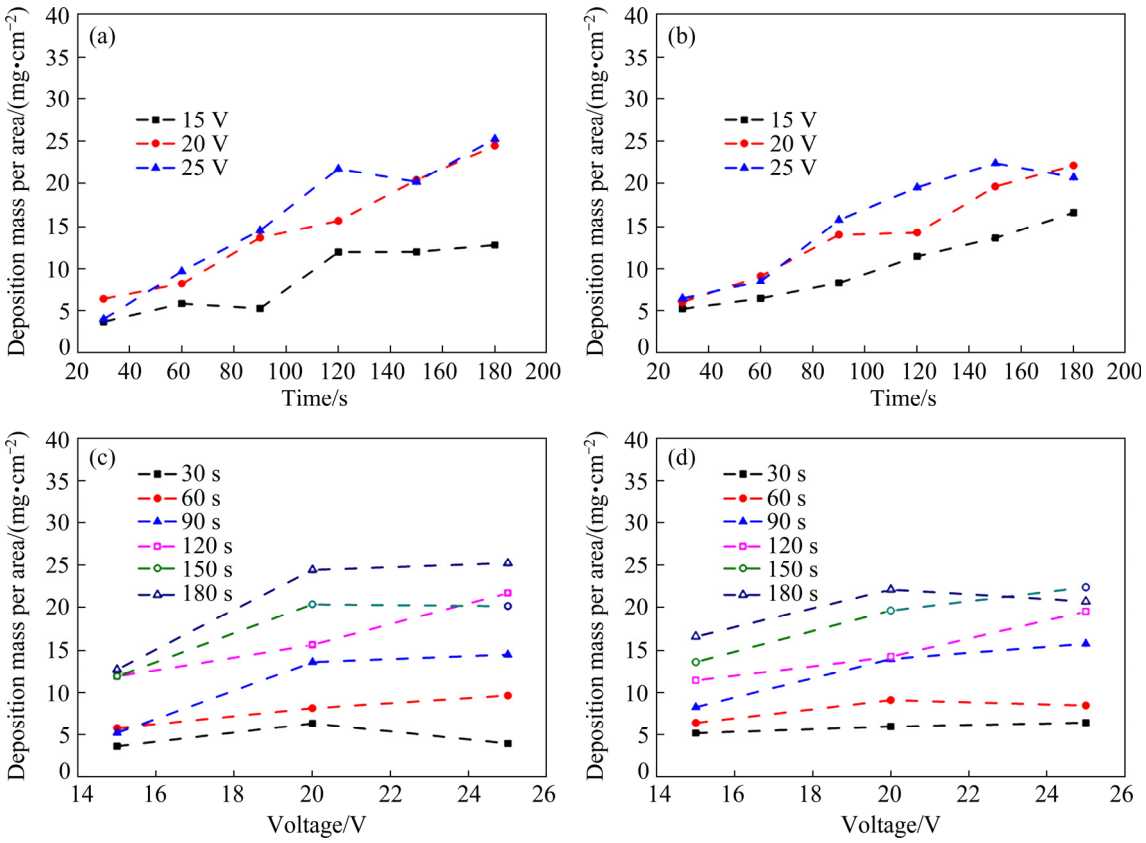

Fig. 2 Deposition mass per area of PEEK (a, c) and P-TN-3 (b, d) coatings under different conditions

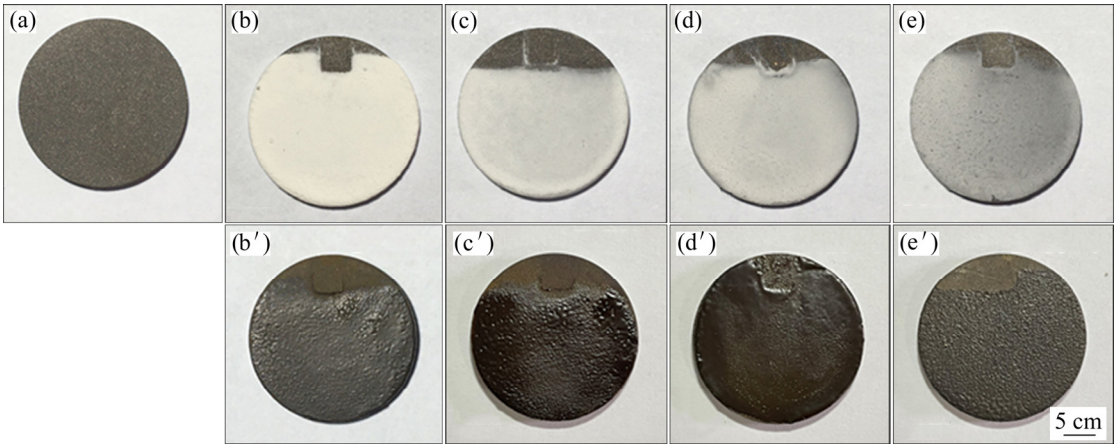

Fig. 3 Macroscopic images of Ti (a), PEEK (b, b′), P-TN-1 (c, c′), P-TN-3 (d, d′), and P-TN-6 (e, e′) coatings before and after heat treatment, respectively

became darker, with the TaN content increased (Figs. 3(c−e)). The crystallized PEEK showed a brownish-yellow color and rough appearance (Fig. 3(b′)), after heat treatment at 390 °C. After introducing the TaN particles into the matrix, the surface of the sample was black-brown and had some lusters. P-TN-1 (Fig. 3(c′)) and P-TN-3 (Fig. 3(d′)) samples with TaN contents of 1.31 wt.% and 3.23 wt.%, respectively, had a much smoother surface than P-TN-6 (Fig. 3(e')) which was composed of 6.25 wt.% TaN, which may all attribute to the agglomeration of large numbers of TaN particles without good dispersion.

2.2 Characterization of powders and coatings

The morphology and microstructure of the raw materials, coatings, and wear counterpart were analyzed with a field-emission scanning electron microscope (FE-SEM, Zeiss, ULTRATM 55, Germany). Field-emission transmission electron microscope (FE-TEM, JEOL JEM−2100F, Japan) with an energy dispersive X-ray spectrometer was used to investigate the compositions. The crystalline structures of the coatings were evaluated by X-ray diffraction (XRD, Rigaku Ultima IV instrument, Japan) at 40 kV with Cu K_α radiation.

The adhesion strength of the composite coatings was measured by using an automated scratch tracer (WS−2005, Lanzhou Zhongke Kaihua Technology Development Co., Ltd., China). Test load varied from 0 to 80 N, loading speed was 80 N/min, scratch length was 5 mm, and the taper angle of the diamond indenter was 120°.

Nanoindentation tests were adopted to evaluate the hardness (H) and elastic modulus (E) of the coatings, and performed with a Berkovich tip by a nanoindenter (G200, Agilent, Santa Clara, CA, USA). The indentations were arranged in arrays of 4 × 4 (i.e. 16 indentations per sample) with a maximum penetration depth of 2 μm by using a depth control mode. The Poisson's ratio of the material was tested and set to be 0.18. The indentations were positioned sufficiently far from each other (50 μm) to neglect the influence of the residual stress field of adjacent indents. And the elastic recovery rate of coating was calculated by Eq. (1) [27]:

$$R=(d_{max}-d_{res})/d_{max}\times 100\% \quad (1)$$

where R is the elastic recovery rate of the coating, d_{max} is the displacement of the maximum load, and d_{res} is the residual displacement of the coating after unloading.

2.3 Tribological tests

The tribological performance of coating was characterized by a reciprocating ball-on-disc tester (MFT−5000, Rtec Instruments Inc., USA). The wear resistance tests of coatings were carried out using the reciprocating-type method in accordance with the ASTM G133—2005 (2016) standard with sliding wear of linear reciprocating ball. ZrO_2 balls with a diameter of 5 mm were used as ceramic counterparts. The average roughness of the ZrO_2 balls was about 0.04 μm. All tests were conducted for 2 h at a room temperature of 20−25 °C and relative humidity of 50%−70%,

under a line contact load of 5 N at a sliding speed of 5 Hz. A Micro-XAM−3D non-contact surface profiler (ADE Corporation, USA) was used to detect 3D topographies and volume loss. The specific wear rate (W, $mm^3 \cdot N^{-1} \cdot m^{-1}$) was calculated by the following equation [28]:

$$W=V/(PL) \quad (2)$$

where V is the wear volume loss of the coating in mm^3, P is the applied load in N, and L is the sliding distance in m. Under each condition, three repeated tests were performed to eliminate the occasionality of the reported results.

3 Results and discussion

3.1 Characterization of coatings

Figure 4 shows the TEM images of PEEK and TaN particles modified with chitosan. As can be seen from Figs. 4(a, b), TaN nanoparticles and chitosan agglomerates were adsorbed to PEEK micro-particles in the suspension. Ta and N elements (Figs. 4(e, g)) may come from TaN, while C and O elements (Figs. 4(f, h)) are from PEEK and chitosan. The distribution of N elements further demonstrated that chitosan was homogeneously dispersed on the PEEK and TaN surfaces. A successful EPD process of TaN/PEEK coating depends greatly on the colloidal procedure. A stable suspension was necessary, and PEEK and TaN particles were dispersed in the suitable medium. PEEK and TaN particles were suitably modified, which effectively prevented flocculation and agglomeration of the particles in this EPD system as shown in Fig. 4.

If a much higher applied electric field is adopted, the particles could not get enough time to find the best position to form a close-packed microstructure. It is also hard to form a uniform and homogeneous coating [29]. Uniform and homogeneous TaN/PEEK coatings (PEEK, P-TN-1, P-TN-3, P-TN-6) were obtained from alcohol-based suspension with a voltage of 20 V during 180 s (Figs. 5(a−d)). The dispersion analysis results of C and Ta elements were shown in Figs. 5(a′−d′). In order to densify the deposited coating, a heat treatment was carried out at 390 °C, and the morphologies were shown in Figs. 5(a″−d″).

Figures 5(a, a′) present the micromorphology and element mapping detail of as-deposited pure PEEK coating. The surfaces of the P-TN-1 and P-TN-3 were much smoother than that of pure PEEK, and TaN was evenly dispersed throughout the surface (Figs. 5(b′, b″, c′, c″)). When the amount of TaN was increased to 6.25 wt.% (P-TN-6) (Fig. 5(d)), obvious agglomeration of TaN particles occurred on the coating surface (Fig. 5(d′)). There is a general thumb rule about suitable specific particle sizes for electrophoretic deposition, and good deposition for a variety of particles has been reported to occur in a range of less than 10 μm [30]. For large particles, the main problem is that they tend to settle due to gravity, the mobility of large

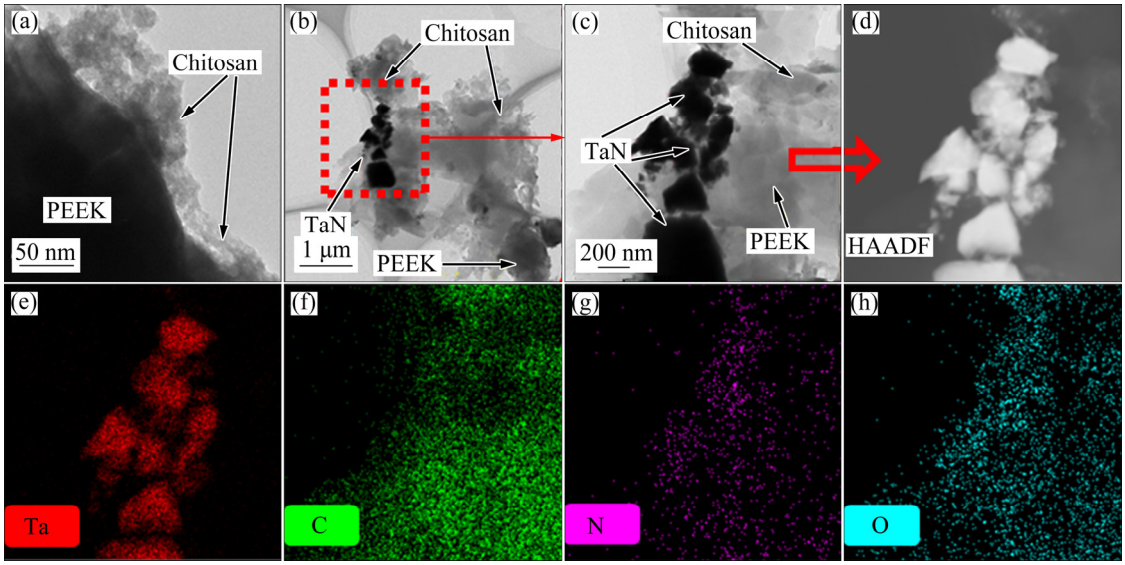

Fig. 4 TEM (a−c) and HAADF-STEM (d) images of PEEK and TaN particles dispersed in solution, and EDX maps of Ta (e), C (f), N (g) and O (h)

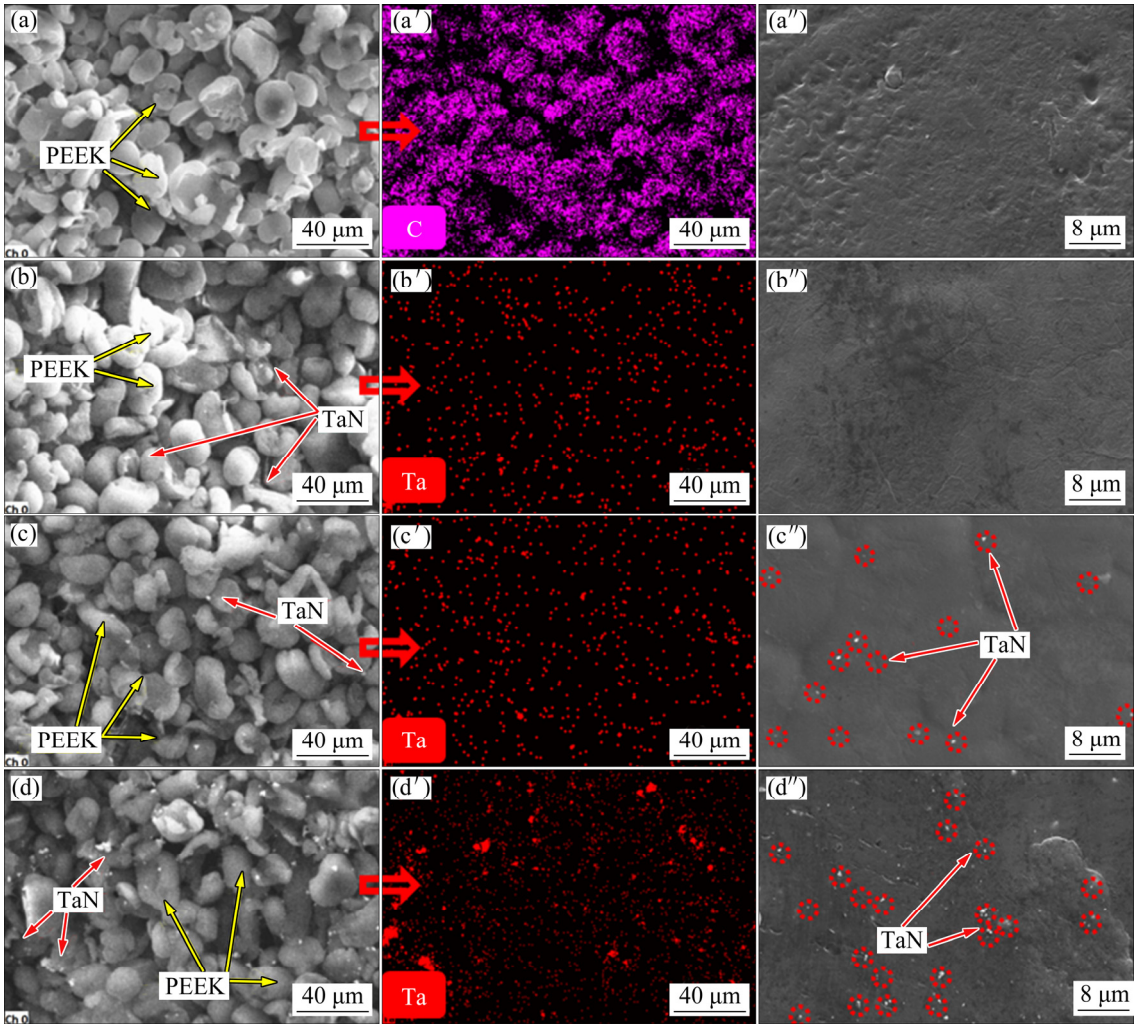

Fig. 5 SEM images of PEEK (a, a″), P-TN-1 (b, b″), P-TN-3 (c, c″), and P-TN-6 (d, d″) coatings before and after heat treatment, respectively, and elemental mappings of C (a′) and Ta (b′−d′)

particles is also lower than that of the small ones, and it is difficult to for large particles to get uniform deposition from a sediment suspension. A large PEEK particle (25 μm) was successfully modified and strongly charged by polycation chitosan, and a uniform coating was obtained.

The cross-section SEM images of the coatings (Figs. 6(a, c)) show that the coating thickness can be increased by introducing TaN nanoparticles under the same deposition condition. The coating thickness increased from 56.8 to 86.8 μm. From the cross-section of P-TN-3, Ta element distribution was relatively uniform in the coating (Figs. 6(c, d, e)). The PEEK and P-TN-3 coatings were all combined well with the titanium matrix. And the heat treatment led to uniform and dense coatings. There was a good bonding between the coating and the substrate, and no obvious cracks were found at the interface.

The X-ray diffraction (XRD) results reveal that heat treatment could improve the crystallinity of the TaN/PEEK coatings. The relative intensity and the peak position of the XRD patterns did shift with the change of TaN amount, which reflected different crystallization behaviors of PEEK (Fig. 7). While the hardness, elastic modulus, adhesion to the substrate, and friction properties of the coating were all up to the crystallization properties of PEEK [31]. Moreover, the crystal peak intensity of PEEK decreased while the TaN particles were introduced under the same heat treatment condition. According to the research of LAI et al [32], the small enhancement could suppress the growth of PEEK crystallites and bring much finer and higher density of crystallites. When the modified nanofillers are incorporated, the spatial suppressing seems to be responsible for the decrease in the inter-planer spacing of the PEEK crystal lattice [33].

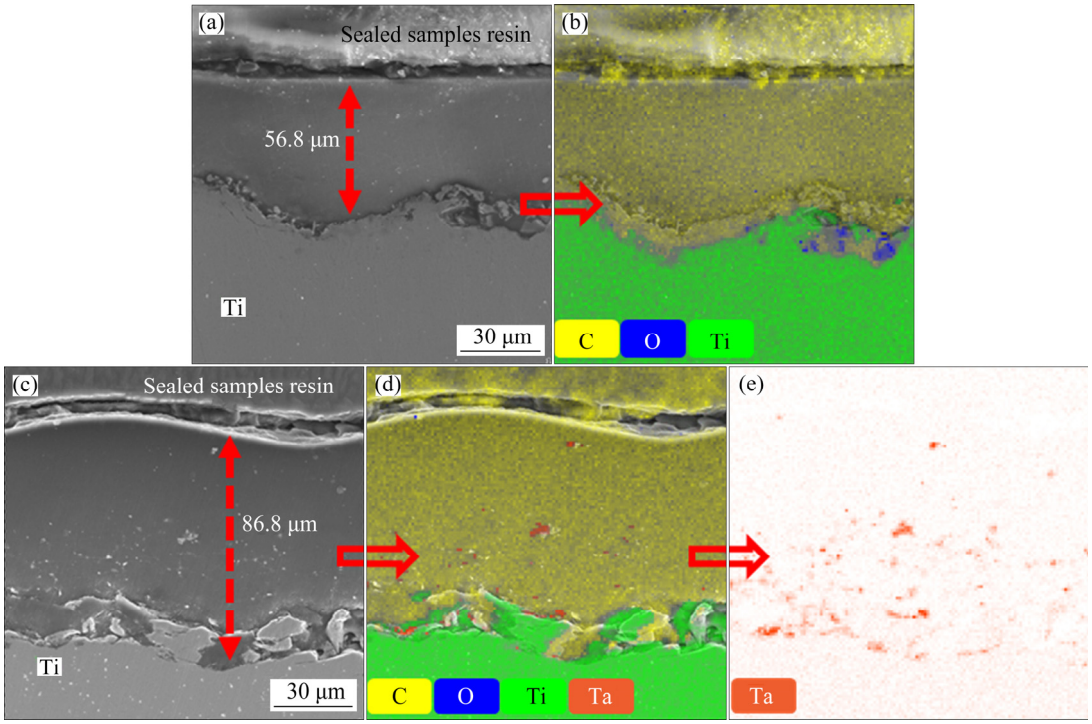

Fig. 6 Cross-section SEM images (a, c) and corresponding EDX elemental mappings (b, d, e) of PEEK (a, b) and P-TN-3 (c−e) coatings

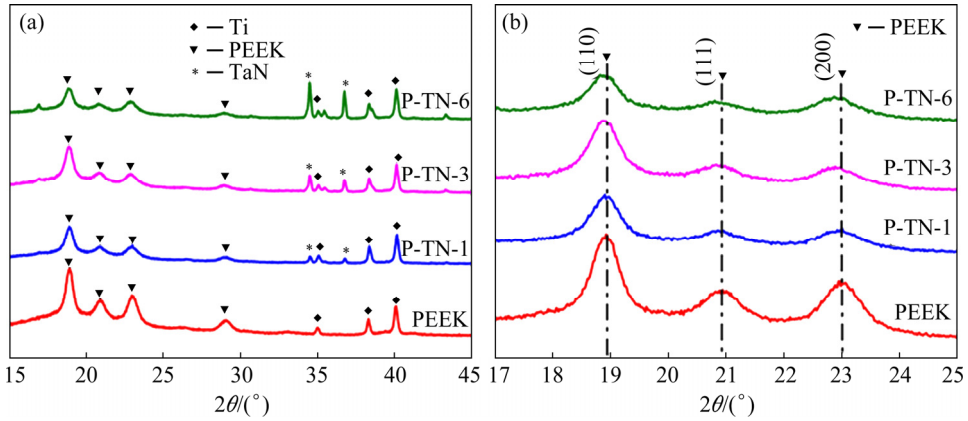

Fig. 7 XRD patterns of different coatings (a) and enlarged views of XRD patterns in 2θ range of 17°−25° (b)

The hardness and elastic modulus properties of coatings were analyzed by a G200 nano-indentation, as shown in Fig. 8. Different contents of TaN nano-particles reinforcement coatings displayed different load/unload−displacement curves, as shown in Fig. 8(a). The elastic recovery rate of the coating was calculated by Eq. (1). The results were organized as follows: P-TN-3 (40.73%) > P-TN-1 (38.32%) > P-TN-6 (36.61%) > PEEK (35.41%). TaN was beneficial to improving the elastic recovery rate of PEEK coating. Among other coatings, the hardness of P-TN-3 was found to increase by 34% to (0.35±0.01) GPa compared to the pure PEEK ((0.26±0.01) GPa). An average hardness of (0.31±0.02) GPa with P-TN-6 was achieved, while that of the P-TN-1 reduced to (0.25±0.02) GPa (close to that of PEEK). TaN as a hard particle plays a strengthening role, thus, the TaN/PEEK hardness was improved. However, excessive TaN would agglomerate and decrease the hardness of the coating (Fig. 8(b)).

Previous studies found that to great impact of the friction coefficient and wear resistance of composite coatings, the ratio of hardness to elastic modulus (H/E) plays an essential role [34]. The structures with a high ratio of H/E can achieve a

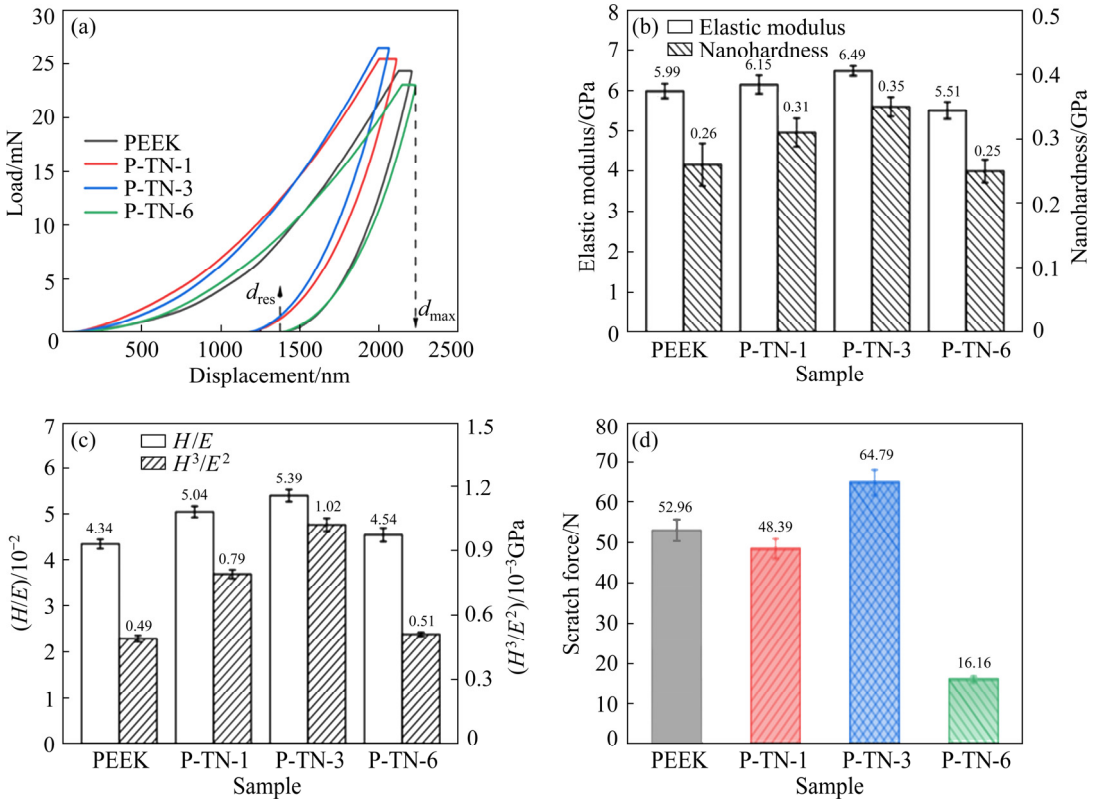

Fig. 8 Load/unload−displacement curves (a), hardness and elastic modulus (b), H/E and H^3/E^2 ratios of different coatings (c), and scratch adhesion test results of different coatings (d)

low friction coefficient and high wear resistance [35]. According to the value obtained by nano-indention, the H/E ratios of different coatings are organized as follows: P-TN-3 (5.39×10^{-2}) > P-TN-1 (5.04×10^{-2}) > P-TN-6 (4.54×10^{-2}) > PEEK (4.34×10^{-2}) (Fig. 8(c)). Particularly, P-TN-3 owns the highest H/E ratio among these four coatings. The P-TN-6 obtained the lowest hardness, but a still higher H/E ratio than that of PEEK.

From measured hardness and elastic modulus values, the H^3/E^2 ratio of coatings were calculated, which exhibited the same ranking law as H/E. The H^3/E^2 ratio of composite coatings spread over an extensive range from 0.49×10^{-3} to 1.02×10^{-3} GPa. In general, P-TN-3 got the highest H^3/E^2 ratio (Fig. 8(c)) as it could distribute the load spreading over a wider area, which reflects the resistance of the coating to plastic deformation [36].

The micro-scratch tests showed that the anti-scratch performance of P-TN-3 was improved by introducing TaN nanoparticles (Fig. 8(d)). The PEEK coating failed under a load of 52.96 N, while the P-TN-3 coating showed a better scratch resistance and failed under a load of 64.79 N. Therefore, P-TN-3 obtained higher H/E and H^3/E^2 ratios, better resistance of plastic deformation, enhanced cracking resistance, and improved scratch resistance. A proper amount of well distributed TaN hard phase could improve the mechanical characteristics of the TaN/PEEK coating, which was expected to own an excellent friction property.

3.2 Tribological properties

The friction coefficient and wear rates, as the two crucial factors for tribological performance, were evaluated. Figure 9(a) illustrates the friction coefficient curves as a function of sliding time. In the initial stage, the titanium suffered from a direct asperity−asperity contact, leading to adherent wear. Initial sliding would cause the fracture of micro-protruded parts between the contacting bodies. The friction coefficient of the titanium was about 0.69. The uneven surface of the coating was smoothened until it matched and balanced, and the friction coefficient increased rapidly to 0.98. The continuous surface wear damage resulted in serious friction and worn conditions, which was consistent with the strong fluctuations in the curve (Fig. 9(a)).

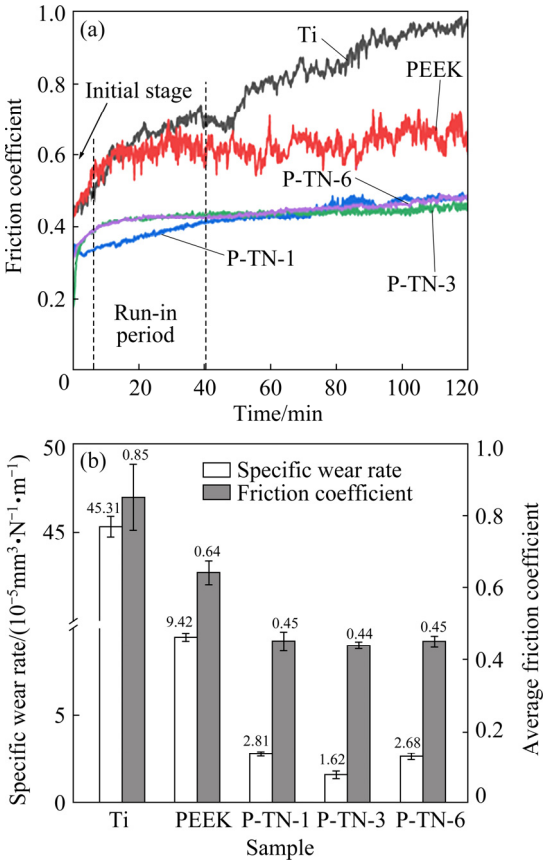

Fig. 9 Friction coefficient curves (a) and average friction coefficient and specific wear rate (b) of different coatings

The friction coefficient of PEEK coating was significantly reduced (0.64). Unlike the plots of other samples, P-TN-1 presented a run-in period. The addition of the TaN nanoparticles decreased the friction coefficient obviously (0.45).

Furthermore, with further increase of the TaN amount in PEEK (P-TN-3), the friction coefficient decreases continuously. The friction coefficient of P-TN-3 was significantly reduced by 48.24% (0.85 to 0.44) compared to that of pure titanium, 31.25% (0.64 to 0.44) compared to that of pure PEEK. It is worth noting that P-TN-3 exhibits the lowest friction coefficient among the composite coatings. The initial friction coefficient of P-TN-3 was similar to that of P-TN-6. After sliding for 60 min, the friction coefficient of P-TN-6 began to increase, while P-TN-3 was stable at 0.44. In a word, the addition of TaN was beneficial to the friction, but the content has little effect on the friction coefficient.

Figure 9(b) shows the specific wear rate of titanium, PEEK, and different TaN/PEEK coatings under the same load. It can be found that the specific wear rate of the TaN/PEEK coating significantly decreased with the addition of TaN. P-TN-3 got the lowest specific wear rate (1.62×10^{-5} $mm^3\cdot N^{-1}\cdot m^{-1}$), which was significantly reduced by 96.42% and 82.80%, compared with titanium and pure PEEK, respectively. What was unusual, P-TN-6 obtained a similar friction coefficient with other composite coatings, but its the specific wear rate increased to 2.68×10^{-5} $mm^3\cdot N^{-1}\cdot m^{-1}$. Namely, there is an optimum value of the TaN amount, too much just as bad as too little, further discussion is in the next section.

To understand the tribological performance, we investigated the morphology and roughness of worn surface. Figure 10 gives the wear tracks SEM and 3D topographies of the titanium, PEEK, P-TN-1, P-TN-3 and P-TN-6 coatings, and Fig. 11 shows the width, depth, and roughness of the wear scar. As can be seen from Figs. 10 and 11, the width, depth, and roughness of the wear scar were sorted by size in descending: Ti > PEEK > P-TN-1 > P-TN-6 > P-TN-3. This trend of declining was as same as the specific wear rate shown in Fig. 9.

The observations of the titanium worn surface were typical furrows and peelings tracks, and abrasive wear is the main wear mechanism. Plenty of wear debris covered the whole titanium surface (Figs. 10(a, a′)), which led to the highest roughness, with a measured value of R_a=(1.32±0.10) μm. The high roughness can be responsible for the fluctuation in friction coefficient plots. The repeated sliding caused severe wear, a 1746.10 μm wide and 156.70 μm deep scar was generated after sliding for 2 h (Fig. 11), and abrasive wear dominated the process.

The depth of wear scar on pure PEEK coating is much shallower (65.10 μm) than that of titanium, with a measured value of R_a=(0.84±0.12) μm (Figs. 10(b′) and 11). There were a few splats of PEEK peeled off, and they were mainly adhesive wear. The irregular furrows indicated that the wear was accompanied by a certain of abrasive wear (Fig. 10(b)). P-TN-1 had a similar worn surface morphology as PEEK, but the depth and width of furrows were significantly reduced, and the surface was relatively flat (Figs. 10(c) and 11). There were few splats peeled off on P-TN-1 surface, coating the surface smoother. The TaN particles supported the surface and improved the bearing capacity of the coating. Meanwhile, the friction contact area and furrows force were reduced.

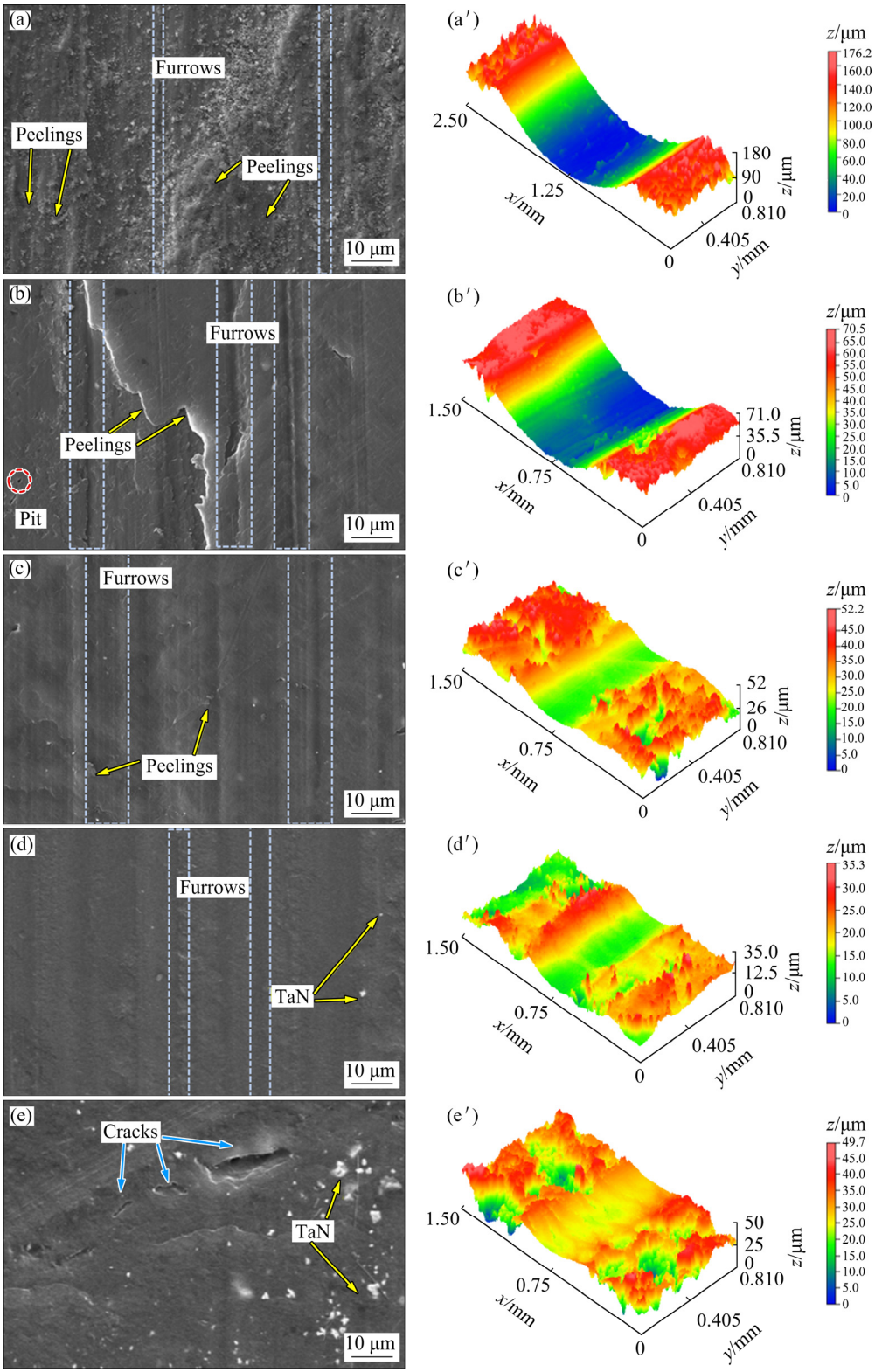

Fig. 10 SEM images (a−e) and three-dimensional (3D) surface topographys (a′−e′) of wear track for different coatings: (a, a′) Ti; (b, b′) PEEK; (c, c′) P-TN-1; (d, d′) P-TN-3; (e, e′) P-TN-6

According to the theory of adhesive friction, the friction force (F) consisted of shear force and furrow force, which could be illustrated by Eq. (3):

$$F=T+P_e=A\tau_b+Sp_e \quad (3)$$

where T is the shear force, and $T=A\tau_b$. A represents the adhesive area, namely the actual contact area, and τ_b is the shear strength of the adhesive junction limit of the soft phase PEEK. P_e is the furrow force,

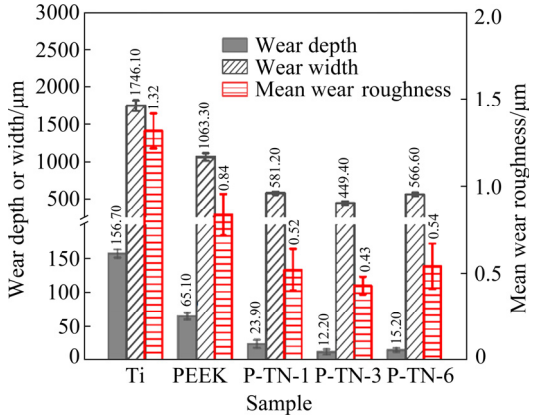

Fig. 11 Wear depth, width, and roughness of different coatings

and P_e=Sp_e. S is the area of furrows, and p_e is the furrow force per unit area [37]. Compared with PEEK, the depth and the furrows amount of P-TN-1 decreased, the corresponding areas of adhesive and furrows were also reduced. The friction force and the friction coefficient of P-TN-1 decreased obviously, which was consistent with the analysis of Fig. 9.

The minimum width (449.40 μm) and the depth (12.20 μm) were obtained for P-TN-3, due to the load bearing capacity improved by the increase of TaN amount. TaN particles could be observed on the worn surface, and high adhesive bonding strength led to less peeling. Minimum friction force resulted in the slightest scratching, keeping with the nanoindentation analysis. P-TN-3 possesses the highest H/E and H^3/E^2 ratios (Fig. 8(c)), which directly reflect the resistance of the coating crack and fracture. The soft PEEK and hard TaN nanoparticles did a synergistic effect to the wear resistance.

As mentioned above, TaN nanoparticles provided a support effect to the coating. However, there was sudden growth in the width, the depth, and the roughness of P-TN-6 wear scar. Obvious cracks could be found on the worn surface, the phenomena of the increased agglomeration of TaN and the reduced furrow numbers all meant that the wear mechanism changed. To further investigate the real wear mechanism, an EDS analysis was performed according to magnified SEM image (Fig. 12).

A group of cracks with the same orientation presented a bamboo-like look, which were perpendicular to the friction direction. As the second

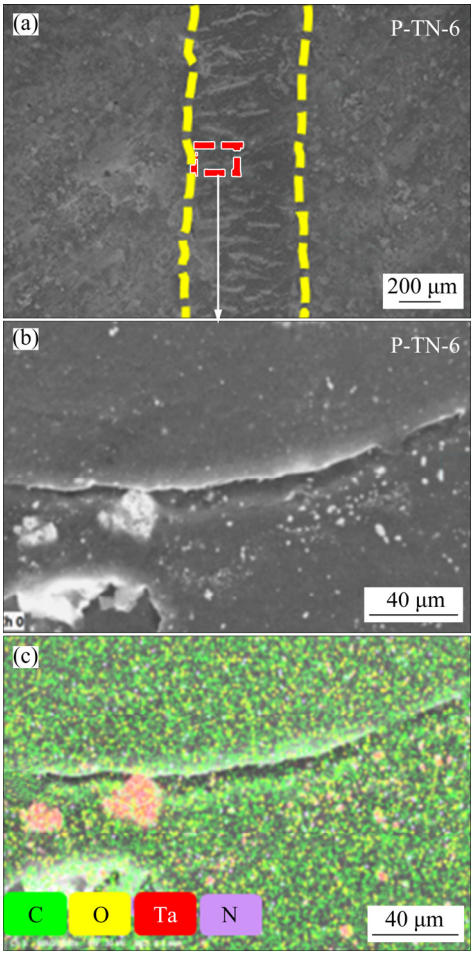

Fig. 12 SEM images (a, b) and elemental mapping of Ta and N elements (c) of P-TN-6 wear scar

phase, the agglomeration of TaN particles would reduce the bond strength of the coating, and crack initiation was also easy to be induced by these hard particles. Under the repeated loading of the friction, the crack grew and propagated. Figure 12(c) illustrates EDS analysis results of the bamboo section, in which the agglomeration of TaN particles was verified.

It is proved that TaN significantly decreased the shear force and furrow force, and the depth of furrows was also reduced. A proper amount of enhancement particles are necessary, and excessive hard particles would cause a scratching effect and worsen the friction condition. The friction force between P-TN-1 and P-TN-3 was decreased, but excessive TaN hard particle agglomeration in P-TN-6 promoted crack initiation and growth.

Besides the low wear rate, an ideal coating should not be over the damage the surface of the matched pair. So, the worn morphologies of friction pairs were also investigated (Fig. 13). An obvious

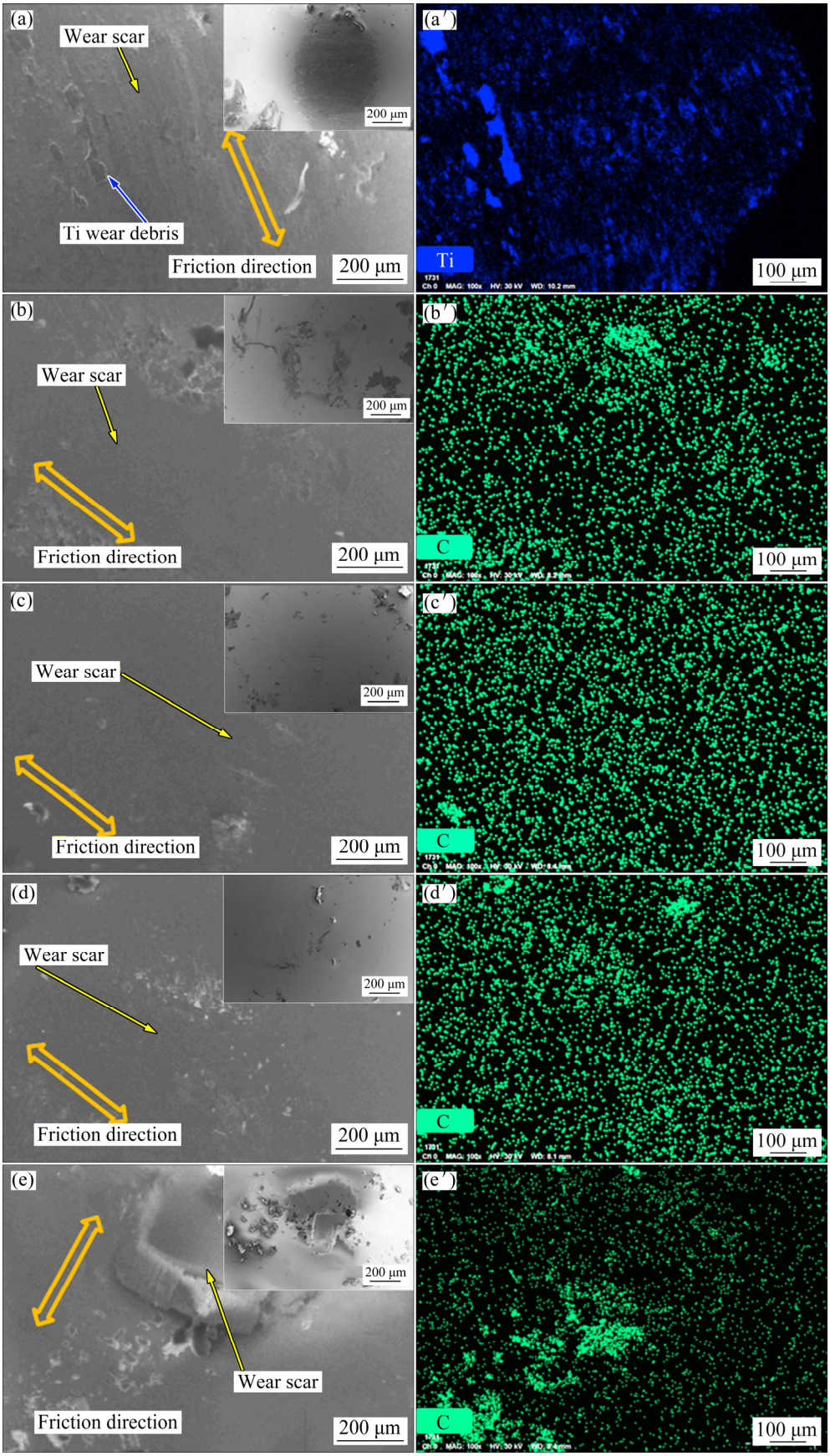

Fig. 13 SEM images of ZrO_2 ball friction pair of different coatings ((a) Ti; (b) PEEK; (c) P-TN-1; (d) P-TN-3; (e) P-TN-6)) and elemental mappings of Ti (a′) and C (b′−e′) elements

wear scar appeared in Fig. 13(a), and a considerable part of titanium was adhesive on the friction pair. A dark area also appeared, which meant that the match ball suffered severe wear.

Because of the low strength, part of PEEK was transferred to the pair ball as shown in Fig. 13(b). Due to the particle reinforcement, the transferred amounts of P-TN-1 and P-TN-3 were less than the that of PEEK (Figs. 13(c, d)). However, there still existed a transfer film, which segregated the direct contact between the two matching pairs, and the abrasion was obviously decreased. This transfer film might be induced by a thermal effect during the friction. When the TaN amount is further increased (P-TN-6), the size and amount of abrasive particles will increase, which goes against the reduction of the friction coefficient of coating, and even damages the surface of pair ball (Fig. 13(e)).

4 Conclusions

(1) TaN/PEEK coating was prepared by EPD, which possessed better adhesion strength and scratch resistance. The PEEK coating failed under a load of 52.96 N, while P-TN-3 coating showed a better scratch resistance and failed under 64.79 N.

(2) TaN nanoparticles reinforced PEEK composite coatings significantly improved the properties of hardness, H/E and H^3/E^2. Particularly, P-TN-3 obtained the highest H/E (5.39×10^{-2}) and H^3/E^2 (1.02×10^{-3} GPa) ratios.

(3) The hybrid tribological coating exhibited excellent wear and lubrication effects. Particularly, P-TN-3 was in the huge boost to the wear resistance. The wear rate was reduced from 9.42×10^{-5} to 1.62×10^{-5} $mm^3\cdot N^{-1}\cdot m^{-1}$. TaN and PEEK synergistically improved the tribological performance of both titanium and friction pairs, and proper amount of TaN enabled the friction coefficient to be greatly reduced by 31.25% to 0.44.

Acknowledgments

This work was supported by the National Key Research and Development Program of China (No. 2018YFB2002000), and the Guangdong Basic and Applied Basic Research Foundation, China (Nos. 2021A515012271, 2019A1515011220, 2020B1515120027).

References

[1] COSTA M M, DANTAS T A, BARTOLOMEU F, ALVES N, SILVA F, MIRANDA G, TOPTAN F. Corrosion behaviour of PEEK or β-TCP-impregnated Ti_6Al_4V SLM structures targeting biomedical applications [J]. Transactions of Nonferrous Metals Society of China, 2019, 29(12): 2523−2533.

[2] PUTRA N E, MIRZAALI M J, APACHITEI I, ZHOU J, ZADPOOR A A. Multi-material additive manufacturing technologies for Ti-, Mg-, and Fe-based biomaterials for bone substitution [J]. Acta Biomaterialia, 2020, 109: 1−20.

[3] BARUI S, PANDA A K, NASKAR S, KUPPURAJ R, BASU S, BASU B. 3D inkjet printing of biomaterials with strength reliability and cytocompatibility: Quantitative process strategy for Ti−6Al−4V [J]. Biomaterials, 2019, 213: 119212.

[4] NAGASE T, TODAI M, HORI T, NAKANO T. Microstructure of equiatomic and non-equiatomic Ti−Nb−Ta−Zr−Mo high-entropy alloys for metallic biomaterials [J]. Journal of Alloys and Compounds, 2018, 753: 412−421.

[5] KIM K T, EO M Y, NGUYEN T T H, KIM S M. General review of titanium toxicity [J]. International Journal of Implant Dentistry, 2019, 5(1): 1−12.

[6] CHAN C W, QUINN J, HUSSAIN I, CARSON L, SMITH G C, LEE S. A promising laser nitriding method for the design of next generation orthopaedic implants: Cytotoxicity and antibacterial performance of titanium nitride (TiN) wear nano-particles, and enhanced wear properties of laser-nitrided Ti_6Al_4V surfaces [J]. Surface and Coatings Technology, 2021, 405: 126714.

[7] ZENG C Y, WEN H, ETTEFAGH A H, ZHANG B, GAO J, HAGHSHENAS A, RAUSH J R, GUO S M. Laser nitriding of titanium surfaces for biomedical applications [J]. Surface and Coatings Technology, 2020, 385: 125397.

[8] ESTHER I, DINAHARAN I, MURUGAN N. Microstructure and wear characterization of AA2124/4wt.%B_4C nano-composite coating on Ti−6Al−4V alloy using friction surfacing [J]. Transactions of Nonferrous Metals Society of China, 2019, 29(6): 1263−1274.

[9] SEN U. Friction and wear properties of thermo-reactive diffusion coatings against titanium nitride coated steels [J]. Materials & Design, 2005, 26(2): 167−174.

[10] COOKE K O, KHAN T I. Effect of thermal processing on the tribology of nanocrystalline Ni/TiO_2 coatings [J]. Emergent Materials, 2018, 1(3): 165−173.

[11] CONRADI M, KOCIJAN A, KOSEC T, PODGORNIK B. Manipulation of TiO_2 nanoparticle/polymer coatings wettability and friction in different environments [J]. Materials, 2020, 13(7): 1702.

[12] HE D Q, PU J B, LU Z B, WANG L P, ZHANG G G, XUE Q J. Simultaneously achieving superior mechanical and tribological properties in WC/aC nanomultilayers via structural design and interfacial optimization [J]. Journal of Alloys and Compounds, 2017, 698: 420−432.

[13] YEO S M. Tribology of polymeric coatings for aggressive

bearing applications [D]. Urbana: University of Illinois at Urbana Champaign, 2013.

[14] FU Q, SAIZ E, RAHAMAN M N, TOMSIA A P. Bioactive glass scaffolds for bone tissue engineering: State of the art and future perspectives [J]. Materials Science and Engineering C, 2011, 31(7): 1245−1256.

[15] CHEN C L, ZHANG Z, ZHAO X W, YE L. Polyoxymethylene/graphene oxide-perfluoropolyether nano-composite with ultra-low friction coefficient fabricated by formation of superior interfacial tribofilm [J]. Composites Part A: Applied Science and Manufacturing, 2020, 132: 105856.

[16] SONG J, LIU Y H, LIAO Z H, WANG S, TYAGI R, LIU W. Wear studies on ZrO_2-filled PEEK as coating bearing materials for artificial cervical discs of Ti_6Al_4V [J]. Materials Science and Engineering C, 2016, 69: 985−994.

[17] THARAJAK J, PALATHAI T, SOMBATSOMPOP N. Recommendations for h-BN loading and service temperature to achieve low friction coefficient and wear rate for thermal-sprayed PEEK coatings [J]. Surface and Coatings Technology, 2017, 321: 477−483.

[18] VISHAL K, RAJKUMAR K, ANNAMALAI V E. Wear and tribofilm characterization of bamboo CNT (B-CNT)-peek composite with incremental blending of submicron synthetic diamond particles [J]. Wear, 2021, 466: 203556.

[19] WANG B, ZHANG K, ZHOU C, REN M, GU Y, LI T. Engineering the mechanical properties of CNT/PEEK nanocomposites [J]. RSC Advances, 2019, 9(23): 12836−12845.

[20] HOU X, HU Y, HU X, JIANG D. Poly (ether ether ketone) composites reinforced by graphene oxide and silicon dioxide nanoparticles: mechanical properties and sliding wear behavior [J]. High Performance Polymers, 2018, 30(4): 406−417.

[21] REN T N, ZHU G M, REN X M, TIAN R J, LI B. Improving interfacial interactions of CF/PEEK composites with sulfonated polyether sulfone [J]. Fibers and Polymers, 2021, 22(1): 231−239.

[22] LENG Y X, SUN H, YANG P, CHEN J Y, WANG J, WAN G J, HUANG N, TIAN X B, WANG L P, CHU P K. Biomedical properties of tantalum nitride films synthesized by reactive magnetron sputtering [J]. Thin Solid Films, 2001, 398: 471−475.

[23] ZHANG Y F, ZHENG Y F, LI Y L, WANG L, BAI Y, ZHAO Q, XIONG X, CHENG Y, TANG Z H, DENG Y, WEI S C. Tantalum nitride-decorated titanium with enhanced resistance to microbiologically induced corrosion and mechanical property for dental application [J]. PLoS One, 2015, 10(6): e0130774.

[24] MOSKALEWICZ T, ZIMOWSKI S, ZYCH A, ŁUKASZCZYK A, RECZYŃSKA K, PAMUŁA E. Electrophoretic deposition, microstructure and selected properties of composite alumina/polyetheretherketone coatings on the Ti−13Nb−13Zr alloy [J]. Journal of the Electrochemical Society, 2018, 165(3): D116− D128.

[25] MOSKALEWICZ T, ZYCH A, KRUK A, KOPIA A, ZIMOWSKI S, SITARZ M, CIENIEK Ł. Electrophoretic deposition and microstructure development of Si_3N_4/polyetheretherketone coatings on titanium alloy [J]. Surface and Coatings Technology, 2018, 350: 633−647.

[26] MOSKALEWICZ T, WARCABA M, ZIMOWSKI S, ŁUKASZCZYK A. Improvement of the Ti−6Al−4V alloy's tribological properties and electrochemical corrosion resistance by nanocomposite TiN/PEEK708 coatings [J]. Metallurgical and Materials Transactions A, 2019, 50(12): 5914−5924.

[27] OLIVER W C, PHARR G M. An improved technique for determining hardness and elastic modulus using load and displacement sensing indentation experiments [J]. Journal of Materials Research, 1992, 7(6): 1564−1583.

[28] ZHAO X Y, ZHANG P, WANG X J, CHEN Y X, LIU H, CHEN L, SHENG Y Y, LI W. In-situ formation of textured TiN coatings on biomedical titanium alloy by laser irradiation [J]. Journal of the Mechanical Behavior of Biomedical Materials, 2018, 78: 143−153.

[29] BESRA L, LIU M L. A review on fundamentals and applications of electrophoretic deposition (EPD) [J]. Progress in Materials Science, 2007, 52(1): 1−61.

[30] WANG C, MA J, CHENG W. Formation of polyetheretherketone polymer coating by electrophoretic deposition method [J]. Surface and Coatings Technology, 2003, 173(2/3): 271−275.

[31] ZHANG C, ZHANG G, VINCENT J, LIAO H L, COSTIL S, CODDET C. Microstructure and mechanical properties of flame-sprayed PEEK coating remelted by laser process [J]. Progress in Organic Coatings, 2009, 66(3): 248−253.

[32] LAI Y H, KUO M C, HUANG J C, CHEN M. On the PEEK composites reinforced by surface-modified nano-silica [J]. Materials Science and Engineering A, 2007, 458(1/2): 158−169.

[33] GOYAL R K, NEGI Y S, TIWARI A N. Preparation of high performance composites based on aluminum nitride/poly (ether–ether–ketone) and their properties [J]. European Polymer Journal, 2005, 41(9): 2034−2044.

[34] LEYLAND A, MATTHEWS A. On the significance of the H/E ratio in wear control: A nanocomposite coating approach to optimised tribological behaviour [J]. Wear, 2000, 246(1/2): 1−11.

[35] NI W Y, CHENG Y T, LUKITSCH M J, WEINER A M, LEV L C, GRUMMON D S. Effects of the ratio of hardness to Young's modulus on the friction and wear behavior of bilayer coatings [J]. Applied Physics Letters, 2004, 85(18): 4028−4030.

[36] CHEN X J, DU Y, CHUNG Y W. Commentary on using H/E and H^3/E^2 as proxies for fracture toughness of hard coatings [J]. Thin Solid Films, 2019, 688: 137265.

[37] WEN S Z, HUANG P. Principles of tribology [M]. Beijing: Tsinghua University Press, 2012: 205. (in Chinese)

TaN 纳米颗粒对电泳沉积 PEEK 涂层显微组织、力学性能和摩擦学性能的影响

曹 琳[1]，张 鹏[1,2]，李双建[1,2]，王启伟[1]，曾大海[1]，
俞传永[1]，李庆阳[1]，廖于文[1]，林志丹[1]，李 卫[1]

1. 暨南大学 先进耐磨蚀及功能材料研究院，广州 510632；
2. 暨南大学 韶关研究院，韶关 512027

摘 要：为解决钛的摩擦、磨损和润滑问题，通过电泳沉积制备一系列 TaN/PEEK(聚醚−醚−酮)涂层，并探讨 TaN 纳米颗粒对涂层显微组织、力学性能和摩擦学性能的影响。结果表明，在 PEEK 涂层中引入 TaN 纳米颗粒可有效提高沉积效率，增强材料抗变形能力，同时还可增加涂层的硬度、弹性模量以及与基底之间的结合强度。与纯 PEEK 涂层相比，P-TN-3 样品的摩擦因数降低 31.25%，耐磨性大幅度提高，其比磨损率由 9.42×10^{-5} 降低到 1.62×10^{-5} $mm^3\cdot N^{-1}\cdot m^{-1}$。电泳沉积制备的复合 TaN/PEEK 涂层均匀分布于钛合金基体表面，且与钛合金基体结合良好，TaN 颗粒可有效提高 PEEK 涂层的强度，为钛合金提供耐磨保护作用。

关键词：聚醚−醚−酮涂层；氮化钽；颗粒强化；显微组织；力学性能；生物摩擦学

(Edited by Wei-ping CHEN)